IEEE Access
Multidisciplinary | Rapid Review | Open Access Journal

Received 9 January 2024, accepted 13 January 2024, date of publication 22 January 2024, date of current version 25 March 2024.

Digital Object Identifier 10.1109/ACCESS.2024.3356586

RESEARCH ARTICLE

An NN-Aided Near-and-Far-Field Classifier via Channel Hankelization in XL-MIMO Systems

JUNG-HWAN KIM[1], DONG-HWAN KIM[2], MUSTAFA OZGER[3], AND WOONG-HEE LEE[1], (Member, IEEE)

[1]Division of Electronics and Electrical Engineering, Dongguk University-Seoul, Seoul 04620, Republic of Korea
[2]Department of Electro-Mechanical Engineering, Korea University, Sejong-si 30019, Republic of Korea
[3]School of Electrical Engineering and Computer Science, KTH Royal Institute of Technology, 114 28 Stockholm, Sweden

Corresponding author: Woong-Hee Lee (woongheelee@dongguk.edu)

This work was supported in part by the Regional Innovation Strategy (RIS) through the National Research Foundation of Korea (NRF) funded by the Ministry of Education (MOE) under Grant 2021RIS-004, and in part by the Institute of Information & Communications Technology Planning & Evaluation (IITP) Grant funded by the Korea Government (MSIT) (Development of integrated interference analysis technology for improving frequency utilization efficiency) under Grant RS-2023-00217885.

ABSTRACT Compared to classical communication systems, sixth-generation (6G) communication requires higher data rates, lower latency, improved energy efficiency, and more diverse users. To satisfy these many requirements, the extremely large-scale massive multiple-input multiple-output (XL-MIMO) system is attracting attention as a promising technology in 6G communication. Depending on the distance between a transmitter and a receiver, the electromagnetic radiation channels in XL-MIMO systems are divided into two models: near-field and far-field channels. The main difference between far-field and near-field is the phase-linearity, resulting in a need for a differentiated system design such as beam management. As a consequence, it is essential to classify near-field and far-field. This paper presents a new neural network (NN)-aided framework for classifying near-field and far-field using the partially captured channel in downlink scenarios in XL-MIMO systems. It is based on the mathematical reasoning that an effective latent space can be constructed with a small amount of data by using the singular values of the channel Hankelization. Briefly, it is to determine the one-hot encoding vector corresponding to each field and learn the singular values of the Hankelized channel matrix. It is noteworthy that this framework operates using the short length of input vectors and the small size of the training dataset. Simulation results show that the proposed method shows the detection rate of about 90% in almost all scenarios. Interestingly, the proposed method shows almost 100% of detection ratio in high SNR environments. It is believed that the proposed method shows superior performance than naïve approaches in various environments, discovering the suitable domain to classify near-field and far-field channels.

INDEX TERMS Extremely large-scale massive MIMO, near-field channel, far-field channel, Hankelization, neural networks, binary classification.

I. INTRODUCTION

Massive multiple-input-multiple-output (MIMO) is one of the most critical technologies in fifth-generation (5G) communication [1], [2]. Massive MIMO with massive antenna arrays in a base station (BS) can improve the spectrum efficiency several times through beamforming or multiplexing [3], [4]. In the future 6G communications, extremely large-scale MIMO (XL-MIMO), which is the evolved version of massive MIMO in terms of the number of antennas, can be a key enabling technology to provide high spectral efficiency, high energy efficiency, and reliable massive access [5], [6].

This enormous increase in the number of antennas requires a change in the analysis of the radiation field of electromagnetic waves. Generally, the radio radiation fields are divided into two areas: near-field and far-field, depending on the Rayleigh distance [7], [8], [13]. The channel in the

The associate editor coordinating the review of this manuscript and approving it for publication was Jad Nasreddine.

TABLE 1. Related works on the studies of near-and-far-field channels. (Our proposed scheme can contribute to these objectives as a preprocessor for classifying near-field and far-field channels.)

Reference	Objective	Description
[3], [7], [8]	Channel estimation	Due to the channel sparsity, many sparse signal processing techniques, such as compressed sensing (CS), are used in channel estimation problems. Most techniques adopt a linear-correlation between dictionaries with many bases and the received signal. Therefore, in a scenario where the near-field is also considered, the dictionary size inevitably becomes much larger. In order to design the dictionary for channel estimation properly, a scheme to determine whether the current channel is the near-field or the far-field is essential.
[9], [10]	Hybrid beamforming	The near-field channel has the distinguishable feature that not only the angle formed by the transceiver but also the distance is reflected in the array response. Conversely, this suggests that high-performance channel estimation can serve to focus the beam on a specific point, rather than radiating it in a specific direction. Based on these characteristics, a technology called beam-focusing, which is an evolved version of existing beamforming, is extensively being developed. From this, it is obvious that the distinction between near-field and far-field channels can be highly helpful in these channel capacity increase technologies.
[11], [12]	Precise localization	Similar to the descriptions above, consideration of the near-field channel leads to similar characteristics in precise localization. A clear analysis of the near-field channel is expected to provide a new direction to existing distance-based or angle-based wireless localization techniques, and the distinction between near-field and far-field channels can greatly contribute to improving wireless localization performance.

near-field area is assumed to be spherical waves, and the array steering vector of the channel under this assumption is associated with distance, as well as the angle between BS and scatterer [14]. On the other hand, the channel in the far-field area is assumed to be a planar wave, and under this assumption, the array steering vector of the channel is associated with only angles between BS and scatterer.

Since the number of antennas is not very large in conventional massive MIMO systems, the Rayleigh distance of up to several meters is negligible [15]. Therefore, existing conventional communication was mainly developed with far-field communication theories and techniques, but near-field communication is essential in the future system since the number of antennas has increased incredibly, and the Rayleigh distance in the radius of a typical 5G cell has increased [15]. As a result, spherical waves should be exploited to realize near-field beam-focusing in XL-MIMO systems to focus signals on a specific location, rather than the conventional far-field beam-steering that steers signals towards a specific angle [16], [17]. In addition, it has been revealed that there is potential in the beam-focusing method in the near-field [9], [10], which is the advanced version of traditional beamforming based on the linearly functional phase in the array response. To alleviate the high pilot overhead in the channel estimation, in current massive MIMO systems, by exploiting the channel sparsity in the angular domain, some compressive sensing-based algorithms have been studied to estimate the high dimensional channels with low pilot overhead [18], [19], [20], [21], [22], [23]. However, the change from massive MIMO to XL-MIMO not only means an increase in antenna number but also leads to a fundamental change in the electromagnetic field structure. Hence, this channel sparsity may not be achievable in XL-MIMO [3].

Overall, Table 1 provides the related works on the studies of near-and-far-field channels, focusing on three categories in wireless communications and some technical considerations by dealing with near-field and far-field channels simultaneously. These research way-forwards in wireless communication systems motivate that it is crucial to classify a near-field channel and a far-field channel in an XL-MIMO system.

In this paper, we present a new simple yet efficient technique based on the low dimensional property that classifies near-field and far-field channels, which is the first trial to the best of our knowledge. Our proposed technique is a new neural network (NN)-aided framework based on the partially captured channel in downlink scenarios in XL-MIMO systems. Considering a single path, the phase domain of the near-field has nonlinear characteristics unlike the far-field. Despite the existence of these characteristics, classifying between the two channels is a difficult task. Moreover, it is hard to classify them with naïve NN techniques due to the similarity between the distributions of near-field and far-field channels. Therefore, we devise new characteristics by using Hankelization and singular value extraction, developing a new suitable domain to classify the near-field and far-field channels. It is based on the mathematical fact that the rank of a Hankelized far-field channel is equal to the channel sparsity, whereas near-field channels do not meet this low rank property due to phase non-linearity. We set the input and output of our proposed NN model to singular values of Hankelized matrices and one-hot encoding vectors, respectively. It demonstrates exceptional performance in classifying near-field and far-field while using smaller sizes of training dataset and pilot symbols than the naïve NN technique.

The remainder of this paper is organized as follows: Section II presents the system model and problem formulation. In Section III, we introduce our proposed method to classify near-field and far-field channels using the NN model. In Section IV, we provide numerical results to demonstrate the superiority of our proposed algorithm in the aspects of various environments. Finally, Section V presents the concluding remarks.

The following notations will be used throughout this paper.

- L: the number of multipaths.
- N: the number of antennas.
- P: the number of pilot symbols.
- K: the index-spacing of pilot symbols. (For convenience, we set $N = PK$.)

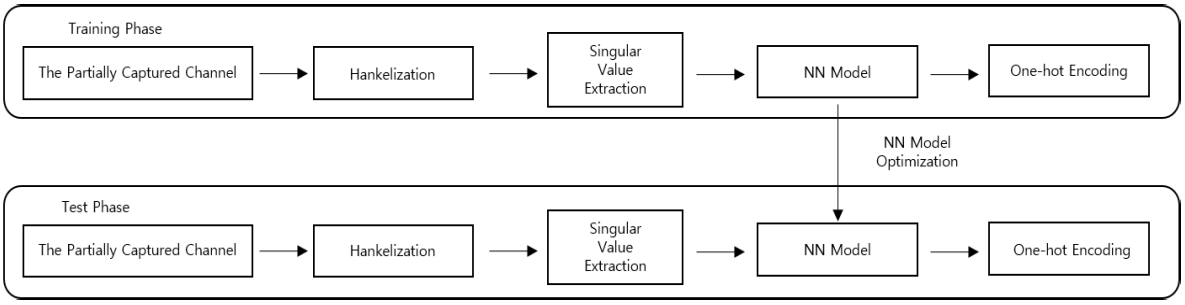

FIGURE 1. Block diagram of the concept of the proposed neural network.

- $\mathbf{h} \in \mathbb{C}^{N\times 1}$: A spatial channel whose length is N.
- $\mathbf{h}_p \in \mathbb{C}^{P\times 1}$: the partially estimated channel of $\mathbf{h}$ via P pilot symbols, i.e., $\mathbf{h}_p[p]$ is the estimate of $\mathbf{h}[pK]$ for all $p \in \{1, \cdots, P\}$.
- $\mathbf{H} \in \mathbb{C}^{P_T\times P'_T}$: the Hankelized channel matrix whose row and column dimensions are P_T and P'_T, respectively, made by $\mathbf{h}_p$.
- $\bar{\sigma} \in \mathbb{R}_+^{P_T}$: the vector of singular values of the Hankelized channel matrix $\mathbf{H}$, which is sorted in descending order.
- $\mathbf{e} \in \{[1\ 0]^T, [0\ 1]^T\}$: the one-hot encoding vector representing near-field or far-field channel. (We set the near-field and far-field channels to $[1\ 0]^T$ and $[0\ 1]^T$, respectively.)
- $\mathcal{S}$: the activation function for NNs; at the propagation between the final hidden layer and the output layer, $\mathcal{S}(a) = a$, i.e., the identity function; at other propagations between the adjacent layers, $\mathcal{S}(a) = \frac{e^a - e^{-a}}{e^a + e^{-a}}$, i.e., the hyperbolic tangent function. And, $\mathcal{S}(\mathbf{a}) = (\mathcal{S}(\mathbf{a}[1]), \cdots, \mathcal{S}(\mathbf{a}[P]))^T$ where $\mathbf{a} \in \mathbb{R}^P$ is an arbitrary input vector.
- P_L: the dimension of the latent space.
- $\mathbf{W} \in \mathbb{R}^{P_L\times P_T}$, $\mathbf{W}' \in \mathbb{R}^{2\times P_L}$: the weight matrices for encoding and decoding, respectively.
- $\mathbf{b} \in \mathbb{R}^{P_L}$, $\mathbf{b}' \in \mathbb{R}^2$: the bias vectors for encoding and decoding, respectively.

II. SYSTEM MODEL AND PROBLEM FORMULATION

We consider a downlink scenario of XL-MIMO, where the BS employs a N-element antenna and communicates with a single user, which receives the signal:

$$\mathbf{y} = \mathbf{x}\mathbf{h} + \mathbf{n}, \tag{1}$$

where $\mathbf{y} \in \mathbb{C}^{N\times 1}$ denotes the signal received by the user in N time slots, $\mathbf{h} \in \mathbb{C}^{N\times 1}$ denotes a channel between the BS and the user, $\mathbf{x} \in \mathbb{C}^{N\times N}$ denotes the signal transmitted by the BS in N time slot, and $\mathbf{n} \in \mathbb{C}^{N\times 1}$ denotes the additive white Gaussian noise with zero mean and σ_n^2 representing the variance. Recalling that K and P are the index-spacing and the number of pilot symbols, respectively, and $N = KP$, we use the pK-th rows of $\mathbf{x}$ for all $p \in \{1, \cdots, P\}$, i.e., P time slots, to capture the channel $\mathbf{h}$. For brevity, for all p, we assume that there is a predetermined pilot symbol at the pK-th index of the pK-th row of $\mathbf{x}$ and the remaining elements of these rows are zeros. Thus, we denote the partially estimated channel via these pilot assignments as $\mathbf{h}_p \in \mathbb{C}^{P\times 1}$, i.e., $\mathbf{h}_p[p]$ is the estimate of $\mathbf{h}[pK]$ for all $p \in \{1, \cdots, P\}$.

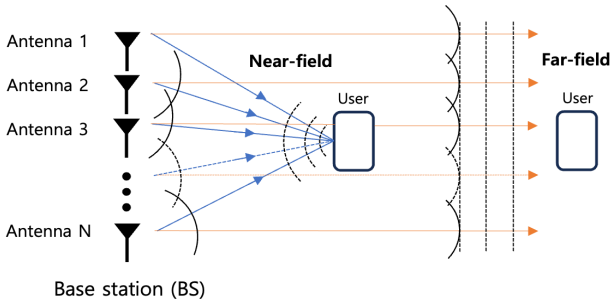

FIGURE 2. Illustration of the description of near-and-far-field.

The radiation field of electromagnetic waves can be divided into near-field and far-field based on the Rayleigh distance $Z = \frac{D^2}{2\lambda}$ where D is the aperture of the antenna and λ is the wavelength, and each region has a different channel model [7]. At this time, it is assumed that there are L scatterers between the single user and the BS. In the near-field, the distance between the BS and the user is shorter than the Rayleigh distance. In the XL-MIMO, assuming that it is a spherical wave, the steering vector is related to the angle and distance. In the far-field, the distance between the BS and the user is longer than the Rayleigh distance. Under the assumption of a planar wave in XL-MIMO, the steering vector is only related to the angle. Under the following assumptions, the definition of the channel model when the user is in the near-field and far-field is as follows.

- Near-field channel model ($\mathbf{h} = \mathbf{h}_{\text{near-field}}$) is written as

$$\mathbf{h}_{\text{near-field}} = \sqrt{\frac{N}{L}} \sum_{l=1}^{L} \alpha_l \mathbf{a}(\theta_l, r_l), \tag{2}$$

where L is the number of path components, N is the number of antennas, α_l represents the l-th path gain and $\theta_l = \frac{2d}{\lambda}\cos(\phi_l)$. Here, $d(= \frac{\lambda}{2})$ is the antenna spacing and $\phi_l \in (0, \pi)$ represents the actual physical angle for the l-th path, i.e., angle of arrival (AoA) between the BS and l-th scatterer. Thus, the steering vector for the l-th path in the near-field, $\mathbf{a}(\theta_l, r_l)$, can be modeled as

follows:

$$\mathbf{a}(\theta_l, r_l) = \sqrt{\frac{1}{N}}[e^{-i\frac{2\pi}{\lambda}(r_l^{(1)}-r_l)}, \ldots, e^{-i\frac{2\pi}{\lambda}(r_l^{(N)}-r_l)}]^H, \tag{3}$$

where $(\cdot)^H$ is the operator of conjugate transpose. In addition, r_l is the distance from the l-th scatterer to the center of the antenna array. The distance from the l-th scatterer to the n-th antenna is $r_l^{(n)} = \sqrt{r_l^2 + d^2\delta_n^2 - 2r_l d\delta_n\theta_l}$ for all l, where $\delta_n = (2n - N - 1)/2$.

- Far-field channel model ($\mathbf{h} = \mathbf{h}_{\text{far-field}}$) is written as

$$\mathbf{h}_{\text{far-field}} = \sqrt{\frac{N}{L}}\sum_{l=1}^{L}\beta_l\mathbf{b}(\theta_l), \tag{4}$$

where β_l is the l-th path gain, and $\mathbf{b}(\theta_l)$ is the steering vector in the far-field, and is as follows:

$$\mathbf{b}(\theta_l) = \sqrt{\frac{1}{N}}[1, e^{-i\pi\theta_l}, \ldots, e^{-i(N-1)\pi\theta_l}]^H. \tag{5}$$

Here, $\theta_l = \frac{2d}{\lambda}\cos(\phi_l)$, and d and ϕ_l are the same as defined in the near-field channel modeling part.

Finally, the objective of this work is to classify whether $\mathbf{h}$ is a near-field or a far-field channel through the partially estimated channel $\mathbf{h}_p$.

III. AN NN-AIDED NEAR-AND-FAR-FIELD CLASSIFIER VIA CHANNEL HANKELIZATION

A. A MATHEMATICAL BACKGROUND: PROPERTY OF HANKELIZED MATRICES

In this section, useful properties of the Hankelized matrix used in the NN model proposed in this paper are examined. The Hankelized matrix for the partially estimated channel $\mathbf{h}_p$, $\mathbf{H} \in \mathbb{C}^{P_T \times P_T'}$ is as follows:

$$\mathbf{H}[i, j] = \mathbf{h}_p[i + j], \tag{6}$$

where P_T and P_T' are the row and column dimensions of $\mathbf{H}$, respectively. To discuss the usefulness of Hankelization, let $\mathbf{H}^*$ be the $\mathbf{H}$, which is made by noise-free the partially captured channel in the far-field channel. Assuming P_T is larger than L, we can find a useful property regarding the low-rank of $\mathbf{H}^*$ as follows:

$$\text{rank}(\lim_{\gamma_{\text{SNR}}\to\infty}\mathbf{H}^*) = L, \tag{7}$$

where γ_{SNR} is signal-to-noise ratio (SNR) in a channel. To validate this, let us take a closer look into an arbitrary row of $\mathbf{H}^*$, denoted by $\mathbf{H}^*[n, :]$ where $n \in \{0, 1, \cdots, P_T - 1\}$. This is represented as follows:

$$\mathbf{H}^*[n, :] = \sqrt{\frac{N}{L}}\left\{\sum_{l=1}^{L}\beta_l e^{-i(n+p)\pi\theta_l}\right\}_{p=0}^{P_T'-1}. \tag{8}$$

As shown above, $\mathbf{H}^*[n, :]$ is a linear combination of L number of P_T'-sized row vectors which are captured from the l-th multipath component of $\mathbf{h}$. For simplicity, we denote this l-th multipath component of $\mathbf{h}$ in $\mathbf{H}^*[n, :]$ as $\mathbf{h}_l^{[n]}$. Naturally, $\mathbf{H}^*[n, :] = \sum_{l=1}^{L}\mathbf{h}_l^{[n]}$. Then, we can easily verify (7) while checking that all rows in $\mathbf{H}^*[n, :]$ have different L bases. Firstly, two row vectors of $\mathbf{h}_l^{[n]}$ and $\mathbf{h}_l^{[m]}$ are linearly dependent where $n, m \in \{0, 1, \cdots, P_T - 1\}$ and $n \neq m$. This is because $\mathbf{h}_l^{[n]}$ can be represented as follow:

$$\mathbf{h}_l^{[n]} = e^{-i\pi(n-m)\theta_l}\mathbf{h}_l^{[m]}, \tag{9}$$

i.e., $\mathbf{h}_l^{[n]}$ is a constant multiple of $\mathbf{h}_l^{[m]}$, and vice versa. Additionally, two row vectors of $\mathbf{h}_l^{[n]}$ and $\mathbf{h}_{l'}^{[n]}$ are linearly independent where $l, l' \in \{0, 1, \cdots, L-1\}$ and $l \neq l'$. Thus, $\text{rank}(\lim_{\gamma_{\text{SNR}}\to\infty}\mathbf{H}^*) = \min(L, P_T)$. Finally, if L is lower than P_T, then (7) is satisfied.

In the near-field channel, since it is non-linear in the angular domain, it is not possible to know that each column of the Hankelized matrix is independent, so the low-rank property cannot be used. However, the non-ideal $\mathbf{H}$ still has valuable information about the ideal $\mathbf{H}^*$. In this work, we use singular values of $\mathbf{H}$ rather than directly using $\mathbf{h}_p$ to classify near-field and far-field channels. This is based on the inference that they can constitute an efficient latent space.

B. A NUMERICAL EVIDENCE: PROPERTY SINGULAR VALUES OF HANKELIZED MATRICES

In order to show that our approach can make an efficient latent space, we will provide some evidence by numerical analysis about the rationale of the utilization of singular values of Hankelized matrices. Fig. 3 shows the histogram of the original channel, the fast Fourier transform (FFT) processed channel, and the singular values of the Hankelized matrices of the the partially captured channel in the near-field and far-field. The difference between the near-field and far-field distributions in the absolute and angle values of the original channel is small, and the difference between the near-field and far-field distributions in the angle values of the FFT processed channel is also small. However, since the difference between the near-field and far-field distributions when using the absolute value of the FFT processed channel and the singular values of the Hankelized matrices of the the partially captured channel seems meaningful, the NN model for channel classification is aimed in this paper.

In addition, Fig. 4 shows the singular values of the Hankelized matrices of the partially captured channel are meaningful. The t-distributed stochastic neighbor embedding (t-SNE) is a nonlinear dimensionality reduction system that converts high-dimensional data into low-dimensional data [24]. As a result of reducing the near-field and far-field high-dimensional datasets to two dimensions, we can see that the shared near-field and far-field datasets as proposed in the paper have better clustering results than the others.

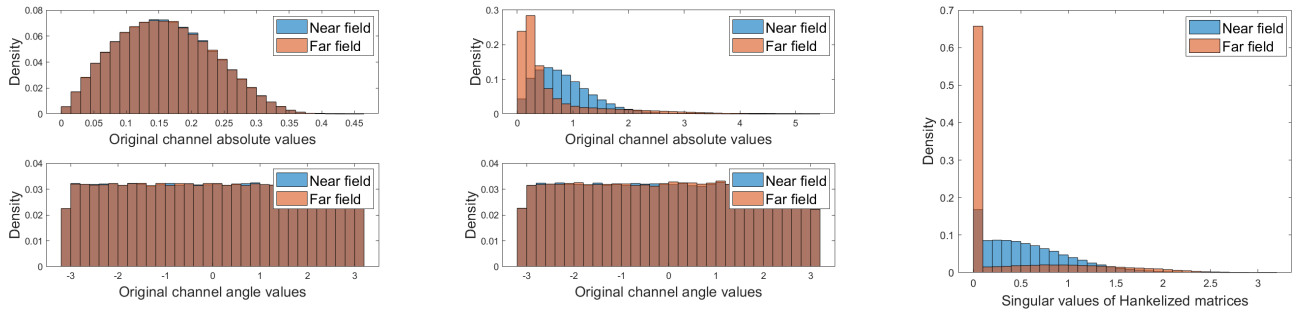

(a) Original channel. (b) FFT processed channel. (c) Singular values of Hankelized matrices.

FIGURE 3. Histograms of utilizable data from near-field and far-field channels.

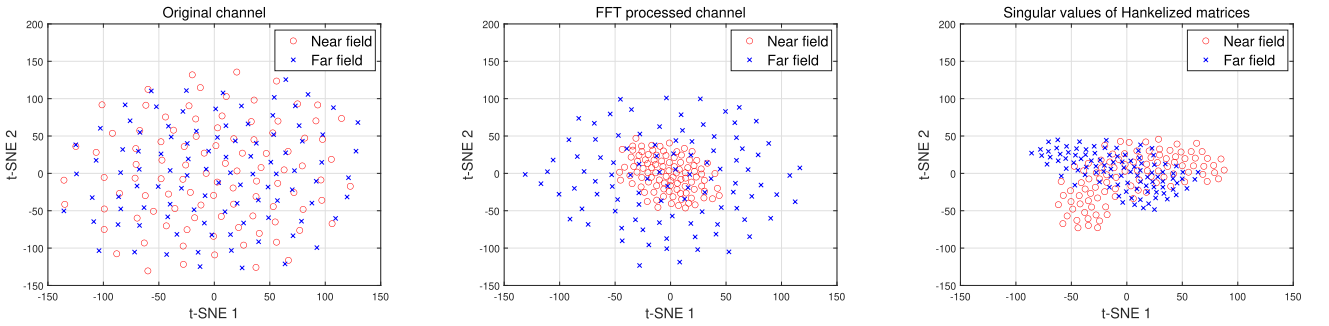

(a) Original channel. (b) FFT processed channel. (c) Singular values of Hankelized matrices.

FIGURE 4. Data visualization based on t-SNE analysis.

C. DESIGN OF THE PROPOSED NN FRAMEWORK

Now, we propose a harmonized design with Hankelization and NN utilization to seek the low-dimensional space to represent the complex channel data.

We define $\mathcal{E}_\theta$ as the encoding function where the parameter θ is $\{\mathbf{W}, \mathbf{b}\}$, i.e., $\mathcal{E}_\theta(\bar{\sigma}) = \mathcal{S}(\mathbf{W}\bar{\sigma} + \mathbf{b})$. In addition, we define $\mathcal{D}_{\theta'}$ as the decoding function where the parameter θ' is $\{\mathbf{W}', \mathbf{b}'\}$, i.e., $\mathcal{D}_{\theta'}(\mathcal{E}_\theta(\bar{\sigma})) = \mathcal{S}(\mathbf{W}'\mathcal{E}_\theta(\bar{\sigma}) + \mathbf{b}')$. Finally, we can define the optimized encoding and decoding NN models, denoted by $\mathcal{E}_{\theta*}$ and $\mathcal{D}_{\theta'*}$, respectively, as follows:

$$\{\mathcal{E}_{\theta*}, \mathcal{D}_{\theta'*}\} = \arg\min_{\mathcal{E}_\theta, \mathcal{D}_{\theta'}} \frac{1}{M} \sum_{i=1}^{M} ||\mathbf{e}^{(i)} - \mathcal{D}_{\theta'}(\mathcal{E}_\theta(\bar{\sigma}^{(i)}))||_2^2, \quad (10)$$

where M and (i) are the number and the index of the training dataset, respectively. As shown in (10), we set the mean squared error (MSE) as a loss function. Let Θ be the entire model parameters, i.e., $\Theta := \theta \cup \theta' = \{\mathbf{W}, \mathbf{W}', \mathbf{b}, \mathbf{b}'\}$, we choose the stochastic gradient descent (SGD) as an optimizer that the update rule for the model parameter $\Theta^{(t)}$ at iteration t is as follows:

$$\Theta^{(t+1)} = \Theta^{(t)} - \eta \sum_{i \in \mathcal{B}_t} \nabla_\Theta \left(\frac{1}{M_B} \sum_{i=1}^{M_B} ||\mathbf{e}^{(i)} - \mathcal{D}_{\theta'}(\mathcal{E}_\theta(\bar{\sigma}^{(i)}))||_2^2 \right), \quad (11)$$

where M_B and $\mathcal{B}_t$ are the mini-batch size and the set containing the indices of the input/output pairs in the current mini-batch, respectively. Also, η and ∇_Θ denote the learning rate related to the step size to the update Θ and the gradient operator with respect to Θ, respectively. Through the procedures of (10) and (11), we can optimize the fully-connected (FC) NN model.[1] Now, we can use the optimized NN model for the hypothesis testing of binary classification as follows:

$$\tilde{\mathbf{e}}[0] \underset{near-field}{\overset{far-field}{\lessgtr}} \tilde{\mathbf{e}}[1], \text{ where } \tilde{\mathbf{e}} = \mathcal{E}_{\theta*}(\mathcal{D}_{\theta'*}(\bar{\sigma})). \quad (12)$$

Algorithm 1 shows the procedure of the proposed method.

IV. SIMULATION RESULTS

In this section, we will compare the performance of our proposed NN-based scheme with the deep learning-based model using absolute values of 1) the original channel and 2) the FFT-processed channel. Table 2 summarizes the parameter values of the simulation setting.

Fig. 5 shows the near-field and far-field channel classification accuracy of the proposed NN model using the confusion matrix. Here, target-class and output-class mean the ground-truth and the estimate, respectively. For instance, the percentages for accuracy of correctly and incorrectly

[1]For simplicity, the description of the NN model design throughout this section is based on a single hidden layer, but it is obvious that deeper hidden layers can be made by multiple encoding/decoding function parameters, i.e., $\{\theta_i\}_{i=1}^d$ and $\{\theta_i'\}_{i=1}^d$, where d, θ_i and θ_i' are the depth of the NN model, the i-th encoding and decoding function parameter.

Algorithm 1 The Procedure of Proposed Neural Network

[*Training phase*]
Collect the training dataset, i.e., the captured channel $\mathbf{h}_p^{(i)}$ and the one-hot encoding vector $\mathbf{e}^{(i)}$ for all $i \in \{1, \cdots, M\}$.
for $i \leftarrow 1$ to M **do**
    Transform $\mathbf{h}_p^{(i)}$ to $\mathbf{H}^{(i)}$.
    Extract the vector consisting of singular values of $\mathbf{H}^{(i)}$ in the descending order, i.e., $\bar{\sigma}^{(i)}$.
end for
Optimize the encoding/decoding functions based on (10), i.e., $\{\mathcal{E}_{\theta^*}, \mathcal{D}_{\theta'^*}\}$, by inputting and outputting $\{\bar{\sigma}^{(1)}, \ldots, \bar{\sigma}^{(M)}\}$ and $\{\mathbf{e}^{(1)}, \ldots, \mathbf{e}^{(M)}\}$, respectively.
[*Test phase*]
Collect the test dataset, i.e., the captured channel $\mathbf{h}_p^{(i)}$ and the one-hot encoding vector $\mathbf{e}^{(j)}$ for all $j \in \{1, \cdots, N\}$.
for $j \leftarrow 1$ to N **do**
    Make the input vector $\bar{\sigma}^{(j)}$ referring steps 4 and 5.
    Guess whether $\mathbf{h}_p^{(i)}$ is near-field or far-field channel via (12).
end for

TABLE 2. Default configuration in the experiments.

Wavelength λ	0.01[m]
# multipaths L	6
# pilot symbols P	32
# antenna N	512
Near-field channel gain α_l	$\mathcal{CN}(0,1)$
Far-field channel gain β_l	$\mathcal{CN}(0,1)$
Angle for the l-th multipath θ_l	$\mathcal{U}(-1,1)$
Distance from l-th scatterer to center of antenna array r_l	$\mathcal{U}(10,80)$
SNR	10 dB
# training dataset	10^4
# test dataset	5×10^4
# hidden layers	2
# neurons per layer	16
Connection type	FC
Loss function	MSE
Optimizer	SGD
Learning rate	10^{-5}
Max. epochs	10^3
Mini-batch size	8

TABLE 3. Detection rate versus the number of the training dataset.

Algorithms \ # training dataset	10^2	10^3	10^4
Proposed neural network	0.8993	0.9471	0.9664
Deep learning-based (original channel)	0.4986	0.5011	0.5049
Deep learning-based (FFT processed channel)	0.6223	0.8324	0.9235

detecting near-field channels are 94.9% and 5.1%, respectively. As shown in this figure, it can be confirmed that the high accuracy of about 94% is obtained in all cases. Based

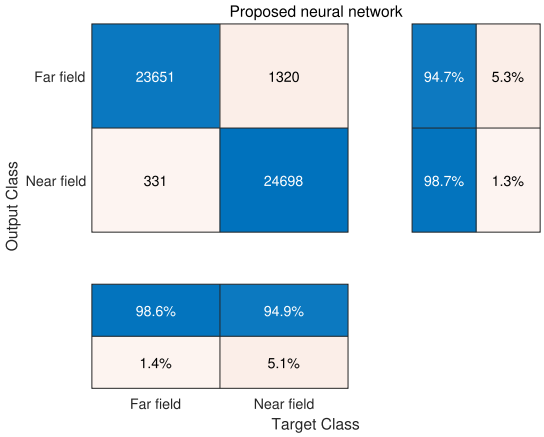

FIGURE 5. Confusion matrix of proposed neural network.

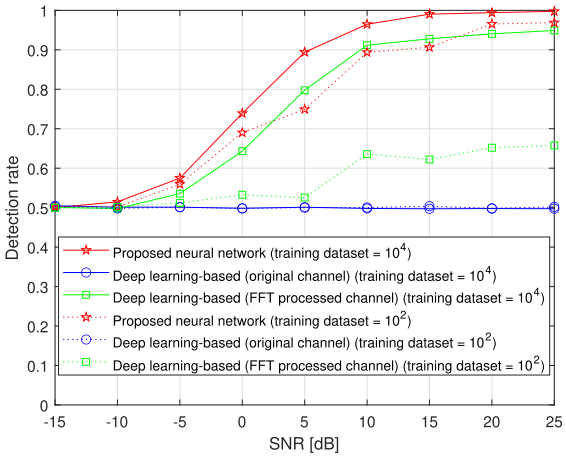

FIGURE 6. Detection rate versus SNR.

on this, it can be seen that the proposed NN model is suitable for classifying near-field and far-field channels; thus, we will examine the detection rate under various conditions.

Table 3 shows the detection rates of near-field and far-field channels according to the number of training dataset. As seen in the figure, it can be seen that the performance of the deep learning-based NN model is obviously inferior when the size of the training dataset is 100. On the other hand, the proposed NN model shows a detection rate of almost 90% or more regardless of the size of the training dataset.

Fig. 6 shows the detection rates of near-field and far-field channels according to SNR. As seen in the figure, it can be seen that the performance of the proposed NN model is superior to those of the deep learning-based NN models. Interestingly, in the case of the proposed NN model, even when the size of the training dataset is 100, it shows a detection rate of about 90% or more from 10 dB, so it shows excellent performance even with a small amount of training dataset.

Fig. 7 shows the detection rates of near-field and far-field channels according to the number of pilot symbols. The figure shows that the detection rate of the proposed NN model is more than 90% when the number of pilot symbols is about

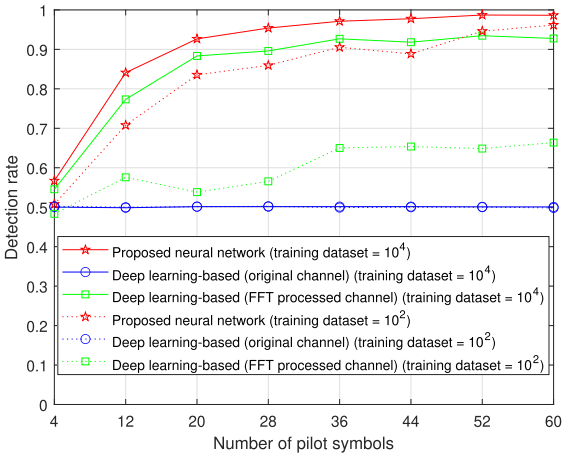

FIGURE 7. Detection rate versus the number of the pilot symbols.

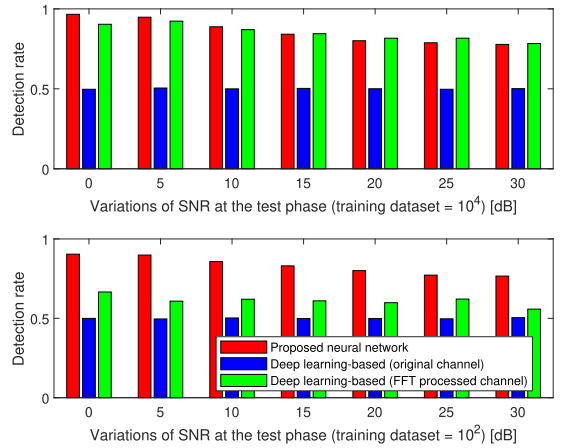

FIGURE 8. Detection rate versus variations of SNR at the test phase.

TABLE 4. Detection rate versus the K-factor.

Algorithms \ K-factor [dB]	2	4	6
Proposed neural network	0.9462	0.9338	0.9261
Deep learning-based (original channel)	0.4987	0.5005	0.4977
Deep learning-based (FFT processed channel)	0.8296	0.8207	0.7429

20 or more. In addition, in the case of the proposed NN model, even when the size of the training dataset is 100, it can be seen that the number of training dataset follows a very similar detection tendency of 10000. Therefore, the proposed NN model presented in this paper can be used regardless of the entire dedicated bandwidth or the allocation pattern of the pilot symbol of the wireless communication system. Unlike naïve NN techniques, it is less affected by the number of training dataset.

Fig. 8 shows performance according to the variations of SNR at the test phase. For instance, if the test of the NN model is conducted in the range of 7.5 dB to 12.5 dB when the NN model is trained at 10 dB SNR, the variation of SNR in the test phase is 5 dB. Fig. 8 shows that the proposed NN model shows a high detection rate in certain variations of SNR despite using a smaller amount of data compared to the naïve deep learning-based model. Also, despite using a small training dataset size, it shows a higher detection rate than naïve NN techniques. Overall, Fig. 8 implies that the proposed NN model shows excellent performance in an environment with different SNRs in training and test phases, which can be a crucial factor in an NN-aided wireless communication system under highly dynamic conditions.

Furthermore, Table 4 shows the detection rates of near-field and far-field channels according to the K-factor that can indicate the power of a dominant path among multipaths. In the situation where the K-factor is 6 dB, the deep learning-based (FFT processed channel) scheme has a detection rate of less than 80%, while the proposed NN model shows more than 90%.

V. CONCLUSION

In this paper, we propose a new framework that classifies near-field and far-field channels by utilizing the singular values of the Hankelized matrices of the partially captured channel in the downlink scenario in XL-MIMO systems. Our proposed framework is based on the mathematical property that if the channel is far-field channel in noise-free environment, it has a low-rank property since it is linear in the angular domain. On the other hand, since the phase of near-field channel is nonlinear, the low-rank property is no longer satisfied; consequently, we use the singular values of Hankelized matrices to distinguish between the near-field and the far-field channels. Simulation results proved that the proposed NN model has excellent classification performance of near-field and far-field channels according to SNR, number of training datasets, and number of pilot symbols. It has been proven that it is a suitable model for classifying near-field and far-field channels. In conclusion, the technique presented in this paper is expected to have potential as a new method for classifying near-field and far-field channels because it shows excellent performance in various conditions despite the small size of the input and training dataset. It is believed that the near-and-far-field classification has lots of opportunities by using it as a preprocessor in representative objectives, e.g., channel estimation, hybrid beamforming, and precise localization, and can be further enhanced by applying more advanced NN models, e.g., transformer.

ACKNOWLEDGMENT

(Jung-Hwan Kim and Dong-Hwan Kim are co-first authors.)

REFERENCES

[1] T. S. Rappaport, S. Sun, R. Mayzus, H. Zhao, Y. Azar, K. Wang, G. N. Wong, J. K. Schulz, M. Samimi, and F. Gutierrez, "Millimeter wave mobile communications for 5G cellular: It will work!" *IEEE Access*, vol. 1, pp. 335–349, 2013.

[2] E. G. Larsson, O. Edfors, F. Tufvesson, and T. L. Marzetta, "Massive MIMO for next generation wireless systems," *IEEE Commun. Mag.*, vol. 52, no. 2, pp. 186–195, Feb. 2014.

[3] M. Cui and L. Dai, "Channel estimation for extremely large-scale MIMO: Far-field or near-field?" *IEEE Trans. Commun.*, vol. 70, no. 4, pp. 2663–2677, Apr. 2022.

[4] H. Elayan, O. Amin, B. Shihada, R. M. Shubair, and M.-S. Alouini, "Terahertz band: The last piece of RF spectrum puzzle for communication systems," *IEEE Open J. Commun. Soc.*, vol. 1, pp. 1–32, 2020.
[5] S. Hu, F. Rusek, and O. Edfors, "Beyond massive MIMO: The potential of data transmission with large intelligent surfaces," *IEEE Trans. Signal Process.*, vol. 66, no. 10, pp. 2746–2758, May 2018.
[6] T. S. Rappaport, Y. Xing, O. Kanhere, S. Ju, A. Madanayake, S. Mandal, A. Alkhateeb, and G. C. Trichopoulos, "Wireless communications and applications above 100 GHz: Opportunities and challenges for 6G and beyond," *IEEE Access*, vol. 7, pp. 78729–78757, 2019.
[7] X. Wei and L. Dai, "Channel estimation for extremely large-scale massive MIMO: Far-field, near-field, or hybrid-field?" *IEEE Commun. Lett.*, vol. 26, no. 1, pp. 177–181, Jan. 2022.
[8] Y. Han, S. Jin, C.-K. Wen, and X. Ma, "Channel estimation for extremely large-scale massive MIMO systems," *IEEE Wireless Commun. Lett.*, vol. 9, no. 5, pp. 633–637, May 2020.
[9] H. Zhang, N. Shlezinger, F. Guidi, D. Dardari, M. F. Imani, and Y. C. Eldar, "Beam focusing for near-field multiuser MIMO communications," *IEEE Trans. Wireless Commun.*, vol. 21, no. 9, pp. 7476–7490, Sep. 2022.
[10] H. Zhang, N. Shlezinger, F. Guidi, D. Dardari, and Y. C. Eldar, "6G wireless communications: From far-field beam steering to near-field beam focusing," *IEEE Commun. Mag.*, vol. 61, no. 4, pp. 72–77, Apr. 2023.
[11] Y. Wang and K. C. Ho, "Unified near-field and far-field localization for AOA and hybrid AOA-TDOA positionings," *IEEE Trans. Wireless Commun.*, vol. 17, no. 2, pp. 1242–1254, Feb. 2018.
[12] J. Liang and D. Liu, "Passive localization of mixed near-field and far-field sources using two-stage MUSIC algorithm," *IEEE Trans. Signal Process.*, vol. 58, no. 1, pp. 108–120, Jan. 2010.
[13] P. Nepa and A. Buffi, "Near-field-focused microwave antennas: Near-field shaping and implementation," *IEEE Antennas Propag. Mag.*, vol. 59, no. 3, pp. 42–53, Jun. 2017.
[14] X. Yin, S. Wang, N. Zhang, and B. Ai, "Scatterer localization using large-scale antenna arrays based on a spherical wave-front parametric model," *IEEE Trans. Wireless Commun.*, vol. 16, no. 10, pp. 6543–6556, Oct. 2017.
[15] M. Cui, Z. Wu, Y. Lu, X. Wei, and L. Dai, "Near-field MIMO communications for 6G: Fundamentals, challenges, potentials, and future directions," *IEEE Commun. Mag.*, vol. 61, no. 1, pp. 40–46, Jan. 2023.
[16] D. Headland, Y. Monnai, D. Abbott, C. Fumeaux, and W. Withayachumnankul, "Tutorial: Terahertz beamforming, from concepts to realizations," *APL Photon.*, vol. 3, no. 5, 2018, Art. no. 51101.
[17] Z. Wu and L. Dai, "Multiple access for near-field communications: SDMA or LDMA?" *IEEE J. Sel. Areas Commun.*, vol. 41, no. 6, pp. 1918–1935, Jun. 2023.
[18] J. Rodríguez-Fernández, N. González-Prelcic, K. Venugopal, and R. W. Heath, "Frequency-domain compressive channel estimation for frequency-selective hybrid millimeter wave MIMO systems," *IEEE Trans. Wireless Commun.*, vol. 17, no. 5, pp. 2946–2960, May 2018.
[19] J. Lee, G.-T. Gil, and Y. H. Lee, "Channel estimation via orthogonal matching pursuit for hybrid MIMO systems in millimeter wave communications," *IEEE Trans. Commun.*, vol. 64, no. 6, pp. 2370–2386, Jun. 2016.
[20] Z. Gao, C. Hu, L. Dai, and Z. Wang, "Channel estimation for millimeter-wave massive MIMO with hybrid precoding over frequency-selective fading channels," *IEEE Commun. Lett.*, vol. 20, no. 6, pp. 1259–1262, Jun. 2016.
[21] C. Huang, L. Liu, C. Yuen, and S. Sun, "Iterative channel estimation using LSE and sparse message passing for mmWave MIMO systems," *IEEE Trans. Signal Process.*, vol. 67, no. 1, pp. 245–259, Jan. 2019.
[22] X. Wei, C. Hu, and L. Dai, "Deep learning for beamspace channel estimation in millimeter-wave massive MIMO systems," *IEEE Trans. Commun.*, vol. 69, no. 1, pp. 182–193, Jan. 2021.
[23] X. Gao, L. Dai, S. Zhou, A. M. Sayeed, and L. Hanzo, "Wideband beamspace channel estimation for millimeter-wave MIMO systems relying on lens antenna arrays," *IEEE Trans. Signal Process.*, vol. 67, no. 18, pp. 4809–4824, Sep. 2019.
[24] L. van der Maaten and G. Hinton, "Visualizing data using t-SNE," *J. Mach. Learn. Res.*, vol. 9, no. 11, pp. 2579–2605, 2008.

JUNG-HWAN KIM received the B.S. degree in electro-mechanical engineering from Korea University, Sejong-si, Republic of Korea, in 2024. He is currently pursuing the M.S. degree with the Division of Electronics and Electrical Engineering, Dongguk University, Seoul, Republic of Korea. His research interests include signal processing and machine learning in wireless communications.

DONG-HWAN KIM is currently pursuing the B.S. degree in electro-mechanical engineering with Korea University, Sejong-si, Republic of Korea. His research interests include signal processing and machine learning in wireless communications.

MUSTAFA OZGER received the B.Sc. degree in electrical and electronics engineering from Middle East Technical University, Ankara, Turkey, in 2011, and the M.Sc. and Ph.D. degrees in electrical and electronics engineering from Koc University, Istanbul, Turkey, in 2013 and 2017, respectively. He is currently a Senior Researcher with the KTH Royal Institute of Technology, Stockholm, Sweden, and serves as one of the technical coordinators of the EU Celtic Next 6G-SKY Project. His research interests include 3D wireless networks and the Internet of Things.

WOONG-HEE LEE (Member, IEEE) received the B.S. degree in electrical engineering from the Korea Advanced Institute of Science and Technology (KAIST), Daejeon, South Korea, in 2009, and the Ph.D. degree in electrical engineering from Seoul National University, Seoul, Republic of Korea, in 2017. From 2017 to 2019, he was an Experienced Researcher with Advanced Standard Research and Development Laboratories, LG Electronics Inc., Seoul. From 2019 to 2020, he was a Postdoctoral Researcher with the Department of Communication Systems, KTH Royal Institute of Technology, Stockholm, Sweden. From 2020 to 2021, he was an Experienced Researcher with Ericsson Research, Stockholm. From 2021 to 2024, he was an Assistant Professor at the Department of Control and Instrumentation Engineering, Korea University, Sejong-si, Republic of Korea. Since March 2024, he has been an Assistant Professor with the Division of Electronics and Electrical Engineering, Dongguk University, Seoul. His research interests include signal processing, machine learning, and game theory in wireless communications.